# Reinvestigation of the high-spin level structure of $^{92}$Nb: Excitations across the $Z = 38$ and $N = 50$ closed shells

Y. Zheng (郑云),[1] Y. H. Wu (吴义恒),[1,2] X. G. Wu (吴晓光),[1,*] C. B. Li (李聪博),[1] L. H. Zhu (竺礼华),[3,4,†] T. X. Li (李天晓),[1] P. W. Luo (罗朋威),[1,5] G. S. Li (李广生),[1] C. Y. He (贺创业),[1] H. W. Li (李红伟),[1] S. P. Hu (胡世鹏),[1,5] J. J. Liu (刘嘉健),[1] J. L. Wang (汪金龙),[1] S. H. Yao (姚顺和),[1] Q. M. Chen (陈启明),[1] J. Zhong (钟健),[1] J. B. Lu (陆景彬),[6] K. Y. Ma (马克岩),[6] and D. Yang (杨东)[6]

[1]*China Institute of Atomic Energy, Beijing 102413, People's Republic of China*
[2]*School of Physics and Electrical Engineering of An Qing Normal University, Anqing 246133, People's Republic of China*
[3]*School of Physics and Nuclear Energy Engineering, Beihang University, Beijing 100191, People's Republic of China*
[4]*Beijing Advanced Innovation Center for Big Data-Based Precision Medicine, Beihang University, Beijing 100083, People's Republic of China*
[5]*College of Physics Science and Technology, Shenzhen University, Shenzhen 518060, People's Republic of China*
[6]*College of Physics, Jilin University, Changchun 130012, People's Republic of China*

(Received 23 January 2019; published 29 July 2019)

High-spin states in $^{92}$Nb have been investigated by using in-beam $\gamma$ ray spectroscopy with the $^{82}$Se($^{14}$N, 4n)$^{92}$Nb reaction at a beam energy of 54 MeV. The positive-parity decay sequences above the previously known state $13^+$ have been extended to $I^\pi \geqslant (20^+)$ by adding nineteen new $\gamma$ rays. The level structures in $^{92}$Nb have been interpreted in terms of the shell model calculations performed in the configuration space $\pi(1f_{5/2}, 2p_{3/2}, 2p_{1/2}, 1g_{9/2})$ for the protons and $\nu(2p_{1/2}, 1g_{9/2}, 1g_{7/2}, 2d_{5/2})$ for the neutrons. The calculated results show that the inclusion of proton core excitation relative to the $Z = 38$ subshell closure and neutron particle-hole excitation for the $N = 50$ shell closure are essential to adequately describe the experimental high-spin states at $I \approx (18\text{–}20)\hbar$ with excitation energies above 8.5 MeV.

DOI: 10.1103/PhysRevC.100.014325

## I. INTRODUCTION

The excited states of nuclei near the $Z \approx 38$ and $N \approx 50$ region have attracted a lot of attention in theoretical and experimental researches [1–38]. It is well known that the low-lying levels in the nuclei with $Z \approx 38$ and $N \approx 50$ have been well described within the shell model framework, by taking $^{88}$Sr as the core and the valence protons occupying the $(2p_{1/2}, 1g_{9/2})$ orbitals [6,12,15,17,39]. Furthermore, the nuclei in the isotonic $N = 51$ chain ($^{89}$Sr, $^{90}$Y, $^{91}$Zr, $^{92}$Nb, $^{94}$Tc, $^{95}$Ru, $^{96}$Rh) have been investigated up to relatively high-spin states [2,3,13,19,21,24,40–43]. With one neutron in the $d_{5/2}$ orbital, high-spin states in the $N = 51$ nuclei can be understood by the interplay between the $(f_{5/2}, p_{3/2}, p_{1/2}) \to g_{9/2}$ proton excitations, $g_{9/2} \to (d_{5/2}, g_{7/2})$ neutron-core excitations or $(d_{5/2} \to g_{7/2})$ neutron excitations, and recouplings of the $g_{9/2}$ valence protons.

For the $^{92}$Nb nucleus, which has three valence protons above the $Z = 38$ subshell closure and one valence neutron above the $N = 50$ subshell closure, we expect that the study of more levels of $^{92}$Nb can provide us with more rich and useful information about the single-particle excitations of both valence protons and neutron as well as the couplings of the core excitation with valence particles. The low-lying levels of $^{92}$Nb were investigated via reactions $^{88}$Zr($^7$Li, $3n$) and $^{91}$Zr($\alpha, t$) [1,3]. The level scheme of $^{92}$Nb was previously known up to the $13^+$ state at 3326 keV and the $11^-$ state at 2203 keV, and was well described within the spherical shell model framework using the model space including the $\pi(p_{1/2}, g_{9/2}) \otimes \nu d_{5/2}$ orbitals [3]. Recently, the low-lying single-particle states in $^{92}$Nb were investigated by Wu *et al.* [36] with the reaction $^{14}$N + $^{82}$Se. However, most positive-parity states above $I = 13\hbar$ were not identified in the previous work. We reanalyzed the data, and here we report newly identified two positive-parity sequences in the $^{92}$Nb nucleus and the comparison with the shell-model calculations.

## II. EXPERIMENTS

The experiment was performed at the HI-13 tandem accelerator in the China Institute of Atomic Energy (CIAE). The high-spin states of $^{92}$Nb were populated via the heavy-ion fusion-evaporation reaction $^{82}$Se($^{14}$N, $4n$)$^{92}$Nb at a beam energy of 54 MeV. The target was a 0.99-mg/cm$^2$-thick isotopically enriched $^{82}$Se metallic foil with a 8.27-mg/cm$^2$ Yb backing to stop the recoiling nuclei. The $\gamma$ rays emitted from the evaporation residues were detected with a multidetector array consisting of nine bismuth germanate (BGO) Compton-suppressed high-purity germanium (HPGe) detectors, whose energy resolutions were about 2.0–2.5 keV at 1.33 MeV, and two planar HPGe detectors with energy resolutions of

*Corresponding author: wxg@ciae.ac.cn
†Corresponding author: zhulh@buaa.edu.cn

 

0.6–0.7 keV at 121.78 keV. These detectors were placed at the forward (40°), 90°, and backward (140°) directions with respect to the beam direction. All HPGe detectors were calibrated for energy and efficiency using the standard energy calibration $\gamma$ lines from the decay of $^{133}$Ba and $^{152}$Eu radioactive sources. A total of $1.5 \times 10^8$ $\gamma$-$\gamma$ coincidence data were accumulated in event-by-event mode. After energy calibration and gain matching for different detectors, the recorded $\gamma$-$\gamma$ coincidence events were sorted into a two-dimensional $E_\gamma$-$E_\gamma$ symmetric matrix by selection on the coincidence time window of 60 ns, and then analyzed using the software package RADWARE [44]. For further strict inspection on $\gamma$-$\gamma$ coincidence relationship, a $E_\gamma$-$E_\gamma$ symmetric matrix with 30 ns time window was also sorted.

In order to obtain information on the multipolarity of $\gamma$ rays, two asymmetric matrices were built, with one axis ($y$ axis) using the $\gamma$ rays detected at all angles, and the other axis ($x$ axis) using those detected at 40° (or 140°) and those detected at 90°. The angular distribution asymmetry (ADO) ratios, defined as $R_{\mathrm{ADO}}(\gamma) = I_\gamma(40^\circ)/I_\gamma(90^\circ)$, were extracted from the $\gamma$-ray coincidence intensities observed by the detectors at either 40° (or 140°) and those at 90° by setting gates on the all-angles axis ($y$ axis). For the present detector geometry, the typical $R_{\mathrm{ADO}}$ value for stretched quadrupole (or $\Delta I = 0$ dipole) transitions was found to be ≈1.4, while for stretched pure dipole transitions it was around 0.7.

## III. THE LEVEL SCHEME

The level scheme of $^{92}$Nb deduced from the present work is shown in Fig. 1. The placement of $\gamma$ rays in the level scheme is based on the $\gamma$-$\gamma$ coincidence relations and $\gamma$-ray intensities. Spin and parity assignments are on the basis of $\gamma$-$\gamma$ directional correlations and deexcitation modes, or are taken from Ref. [3]. The energies, relative intensities, ADO ratios of $\gamma$ rays, and the spin and parity $I^\pi$ assignments of levels are summarized in Table I. The typical coincidence $\gamma$ ray spectra gated on the transitions of $^{92}$Nb are shown in Figs. 2 and 3. Some detailed experimental results are given below.

For sequences 1, 2, and 4 as well as the low-lying part of the level scheme, most of the $\gamma$ rays reported in the previous works [3,36] were confirmed, but the 90-, 123-, 150-, 164-, 194-, 254-, and 357-keV transitions between low-energy levels established by Brown *et al.* [3] were not observed in the present work. From the analysis of the present data, the negative parity sequence 1, which was reported in Ref. [36] to feed into the $11^-$ 167 ns isomer state, was carefully checked in the present analysis. By selecting different coincidence time windows, as shown in Fig. 2(a), the impact of the 167 ns isomer in the coincidence spectrum gated by the 2210-keV $\gamma$ ray is clearly shown by comparison of the relative intensity of 1720.4- and 2086.9-keV transitions; i.e., the relative intensity increases for the prompt 1720.4-keV transition and decreases for the delayed 2086.9-keV transition when the time window becomes narrow. In addition, we have made three major corrections to the negative parity sequence reported in Ref. [36]. First of all, based on the newly identified 597.9-keV transition and the coincidence relationship between 327.8- and 2210.2-keV transitions, as shown in Figs. 2(a) and 3(a), the order of two cascade transitions 1720 → 2210 keV turned out to be reversed. Second, since the 1332.7-keV transition could not be observed in the $\gamma$-ray coincidence spectrum gated on 514.9- and 675.7-keV transitions but it could be seen from that gated on the 580.7-keV transition, as shown in Fig. 2(b)–2(d), the 1332.7-keV transition was changed to a linking transition between the 7323.8- and 5991.8-keV levels. As can be seen from Fig. 2(d), the 1304.9-keV transition could not be observed from the $\gamma$-ray coincidence spectrum gated on the 675.7-keV transition and vice versa. This is also true for the relationship between 628.8- and 1304.9-keV transitions. Therefore, given the coincidence relationship and energy balance between 628.8- and 675.7-keV transitions with the 1304.9-keV transition, the negative parity sequence was modified, as shown in Fig. 1. The newly deduced $R_{\mathrm{ADO}}$ values and the transition selection rules suggest that the spin and parity of 5504.0- and 5991.8-keV levels may be $(14^-)$ and $(15^-)$, respectively. Furthermore, the 628.8- and 1304.9-keV transitions are in coincidence with the 327.8-keV transition but not coincidence with the 1550.5-keV transition. Consequently, there should be a transition or several cascade transitions between 5504.0- and 3325.4-keV levels, but the expected transition was not observed in the present experiment. Thus, these two levels were connected with a dashed line in the present level scheme. Compared with the results reported in Refs. [3,36], the level scheme of $^{92}$Nb was extended significantly in the present work. Nineteen new $\gamma$ rays were identified and assigned in the present level scheme. Particularly, two new positive-parity decay sequences, 3 and 4, were established.

The new sequence 3, built upon the $13^+$ state at 3325.4 keV, was established up to the $I^\pi > (20^+)$ level at 10.74 MeV. This sequence includes twelve transitions. It feeds mainly into the $11^+$ state via the 327.8-keV transition. Based on the dipole character of the 269.3-, 322.2-, 737.9-, 1555.6-, and 1628.5-keV transitions and the quadrupole character of the 2175.6- and 2356.7-keV transitions, the assignments of the $I^\pi = (15^+)$, $(15^+)$, $(16^+)$, $(17^+)$, $(18^+)$, $(18^+)$, $(19^+)$, and $(20^+)$ for the 5501.0-, 5682.1-, 6004.3-, 7632.8-, 7668.7-, 8370.7-, 9926.3-, and 10195.6-keV levels, respectively, were proposed for sequence 3. In addition, the spin of the level at 10736.7 keV was not assigned due to the weak intensity of the 541.1 keV transition and the contaminant $\gamma$ rays. As shown in Fig. 3(a) and 3(b), the members of this sequence, i.e., the above-mentioned transitions and a 541.1-keV transition as well as two $\Delta I = 1$ transitions with energies of 503.5 and 1664.4 keV, are clearly indicated. Besides, several previously known low-lying transitions with energies of 148.2, 711.2, 762.5, 2086.9, and 2286.6 keV are also clearly visible in Figs. 3(a) and 3(b). All of the transitions belonging to sequence 3 are visible in Fig. 3(c), especially two weak $\Delta I = 2$ transitions with energies of 2257.9 and 2293.2 keV. In Fig. 3(d), which is gated on the 1628.5-keV transition, most observed transitions are the same as those in Fig. 3(c) except for two parallel transitions with energies of 2257.9 and 1664.4 keV.

Three new crossover linking transitions with energies of 490.6, 625.2, and 806.5 keV between sequence 2 and

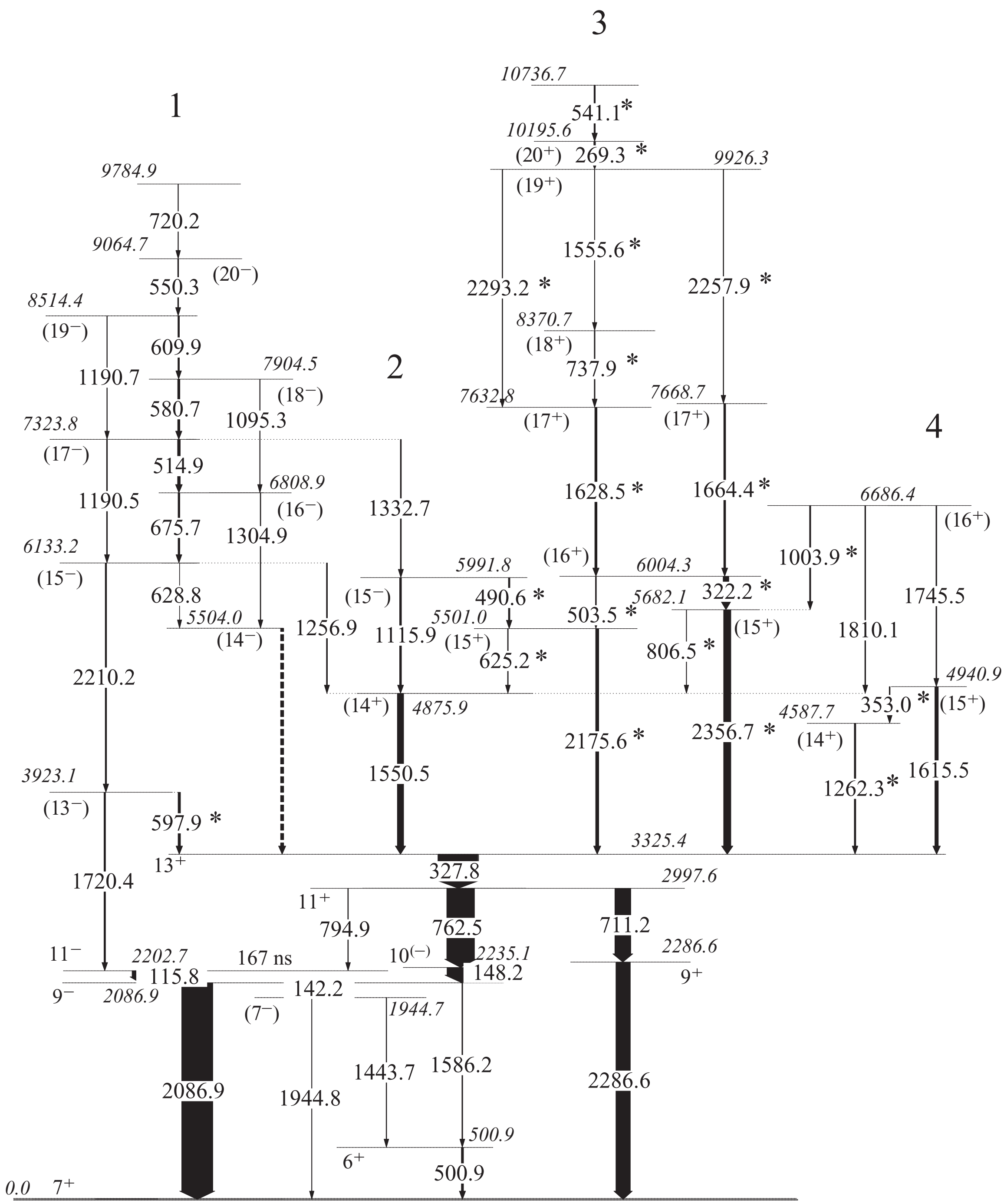


FIG. 1. The level scheme of $^{92}$Nb established from the present work. New $\gamma$ rays are marked with asterisks.

sequence 3 were identified. One can see these three newly identified linking transitions in Fig. 3(a), but only the 806.5-keV transition can be seen in Fig. 3(b) due to their coincidence relationship. In addition, a new crossover linking transition of energy 1003.9 keV was observed to feed the $(15^+)$ state with an energy of 5682.1 keV in sequence 3, and another two new $\gamma$ transitions with energies of 353.0 and 1262.3 keV belonging to sequence 4 were assigned. On the basis of the dipole and quadrupole character of the 1262.3- and 1003.9-keV transitions, respectively, $I^\pi = (14^+)$ and $(17^+)$ for the 4587.7- and 6686.4-keV states were assigned, respectively.

As shown in Fig. 1, there are several $\gamma$ transitions with high energy of about 2 MeV. This is an indication of the excitation of nucleons across a large energy (shell) gap. The observed 1664.4-keV $\gamma$ ray, $(17^+)$ (7668.7 keV) $\rightarrow$ $(16^+)$ (6004.3 keV), may be caused by neutron core excitation of a neutron from the $1g_{9/2}$ orbit to the $1g_{7/2}$ orbit. Other high energy $\gamma$ transitions, such as $(13^-)$ (3923.1 keV) $\rightarrow$ $11^-$ (2202.7 keV), $(15^-)$ (6133.2 keV) $\rightarrow$ $(13^-)$ (3923.1 keV), $(15^+)$ (5682.1 keV) $\rightarrow$ $13^+$ (3325.4 keV), and $(15^+)$ (5501.0 keV) $\rightarrow$ $13^+$ (3325.4 keV) could be attributed to the excitation of protons across the $Z = 38$ subshell gap.

TABLE I. Energies, relative intensities, ADO ratios, and initial and final state spin-parities of $\gamma$-ray transitions assigned to $^{92}$Nb from the present work.

| $E_\gamma$ (keV)[a] | $I_\gamma$[b] | $E_i \rightarrow E_f$ (keV)[c] | $R_{ADO}(\Delta I = 2)$ | $R_{ADO}(\Delta I = 1)$ | $I_i^\pi \rightarrow I_f^\pi$ |
|---|---|---|---|---|---|
| 115.8 | 30.9(6) | 2202.7 → 2086.9 | 1.41(20) | | $11^- \rightarrow 9^-$ |
| 142.2 | 1.9(4) | 2086.9 → 1944.7 | | | $9^- \rightarrow (7^-)$ |
| 148.2 | 88.7(9) | 2235.1 → 2086.9 | | 0.72(4) | $10^{(-)} \rightarrow 9^-$ |
| 269.3 | 5.4(3) | 10195.6 → 9926.3 | | 0.78(13) | $(20^+) \rightarrow (19^+)$ |
| 322.2 | 18.6(4) | 6004.3 → 5682.1 | | 0.84(5) | $(16^+) \rightarrow (15^+)$ |
| 327.8 | 128.7(8) | 3325.4 → 2997.6 | 1.50(4) | | $13^+ \rightarrow 11^+$ |
| 353.0 | 2.9(4) | 4940.9 → 4587.7 | | | $(15^+) \rightarrow (14^+)$ |
| 490.6 | 4.9(3) | 5991.8 → 5501.0 | | 0.68(21) | $(15^+) \rightarrow (15^+)$ |
| 500.9 | 6.9(3) | 500.9 → 0.0 | | | $6^+ \rightarrow 7^+$ |
| 503.5 | 6.8(4) | 6004.3 → 5501.0 | | 0.96(18) | $(16^+) \rightarrow (15^+)$ |
| 514.9 | 8.4(12) | 7323.8 → 6808.9 | | 0.91(17) | $(17^-) \rightarrow (16^-)$ |
| 541.1 | 4.2(4) | 10736.7 → 10195.6 | | | |
| 550.3 | 3.9(2) | 9064.7 → 8514.4 | | 0.69(11) | $(20^-) \rightarrow (19^-)$ |
| 580.7 | 7.1(10) | 7904.5 → 7323.8 | | 0.75(3) | $(18^-) \rightarrow (17^-)$ |
| 597.9 | 1.4(3) | 3923.1 → 3325.4 | | | $(13^-) \rightarrow (13^+)$ |
| 609.9 | 5.7(3) | 8514.4 → 7904.5 | | 0.75(13) | $(19^-) \rightarrow (18^-)$ |
| 625.2 | 2.3(2) | 5501.0 → 4875.9 | | 1.07(21) | $(15^+) \rightarrow (14^-)$ |
| 628.8 | 1.1(5) | 6133.2 → 5504.0 | | | $(15^-) \rightarrow (14^-)$ |
| 675.7 | 5.6(5) | 6808.9 → 6133.2 | | 0.56(17) | $(16^-) \rightarrow (15^-)$ |
| 711.2 | 51.1(5) | 2997.6 → 2286.6 | 1.61(13) | | $11^+ \rightarrow 9^+$ |
| 720.2 | 2.0(2) | 9784.9 → 9064.7 | | | |
| 737.9 | 2.7(4) | 8370.7 → 7632.8 | | 0.69(20) | $(18^+) \rightarrow (17^+)$ |
| 762.5 | 89.1(5) | 2997.6 → 2235.1 | | 0.84(4) | $11^+ \rightarrow 10^-$ |
| 794.9 | 2.0(2) | 2997.6 → 2202.7 | | | $11^+ \rightarrow 11^-$ |
| 806.5 | 1.3(2) | 5682.1 → 4875.9 | | | $(15^+) \rightarrow (14^+)$ |
| 1003.9 | 4.0(3) | 6686.4 → 5682.1 | | 0.77(18) | $(16^+) \rightarrow (15^+)$ |
| 1095.3 | 1.5(3) | 7904.5 → 6808.9 | | | $(18^-) \rightarrow (16^-)$ |
| 1115.9 | 6.0(3) | 5991.8 → 4875.9 | | 0.71(12) | $(15^-) \rightarrow (14^-)$ |
| 1190.5 | 2.9(2) | 7323.8 → 6133.2 | | | $(17^-) \rightarrow (15^-)$ |
| 1190.7 | 1.7(2) | 8514.4 → 7323.8 | | | $(19^-) \rightarrow (17^-)$ |
| 1256.9 | 3.3(5) | 6133.2 → 4875.9 | | 1.0(4) | $(15^-) \rightarrow (14^+)$ |
| 1262.3 | 5.0(7) | 4587.7 → 3325.4 | | 0.81(19) | $(14^+) \rightarrow 13^+$ |
| 1304.9 | 2.3(3) | 6808.9 → 5504.0 | 1.25(34) | | $(16^-) \rightarrow (14^-)$ |
| 1332.7 | 3.3(3) | 7323.8 → 5991.8 | | 1.45(30) | $(17^-) \rightarrow (15^-)$ |
| 1443.7 | 1.8(3) | 1944.7 → 500.9 | | | $(7^-) \rightarrow 6^+$ |
| 1550.5 | 20.2(2) | 4875.9 → 3325.4 | | 0.70(5) | $(14^+) \rightarrow 13^+$ |
| 1555.6 | 1.3(3) | 9926.3 → 8370.7 | | 0.69(38) | $(19^+) \rightarrow (18^+)$ |
| 1586.2 | 3.5(2) | 2086.9 → 500.9 | | | $9^- \rightarrow 6^+$ |
| 1615.5 | 11.0(3) | 4940.9 → 3325.4 | 1.54(25) | | $(15^+) \rightarrow 13^+$ |
| 1628.5 | 7.2(3) | 7632.8 → 6004.3 | | 0.94(22) | $(17^+) \rightarrow (16^+)$ |
| 1664.4 | 4.6(2) | 7668.7 → 6004.3 | | 0.69(38) | $(17^+) \rightarrow (16^+)$ |
| 1720.4 | 4.9(7) | 3923.1 → 2202.7 | 1.32(18) | | $(13^-) \rightarrow 11^-$ |
| 1745.5 | 2.9(2) | 6686.4 → 4940.9 | | | $(16^+) \rightarrow (15^+)$ |
| 1810.1 | 2.9(2) | 6686.4 → 4875.9 | 1.62(26) | | $(16^+) \rightarrow (14^+)$ |
| 1944.8 | 1.2(3) | 1944.7 → 0.0 | | | $(7^-) \rightarrow 7^+$ |
| 2086.9 | 100.0 | 2086.9 → 0.0 | 1.42(8) | | $9^- \rightarrow 7^+$ |
| 2175.6 | 10.0(3) | 5501.0 → 3325.4 | 1.57(20) | | $(15^+) \rightarrow 13^+$ |
| 2210.2 | 4.4(6) | 6133.2 → 3923.1 | 1.74(19) | | $(15^-) \rightarrow (13^-)$ |
| 2257.9 | 1.7(2) | 9926.3 → 7668.7 | | | $(19^+) \rightarrow (17^+)$ |
| 2286.6 | 46.3(6) | 2286.6 → 0.0 | 1.85(21) | | $9^+ \rightarrow 7^+$ |
| 2293.2 | 0.5(1) | 9926.3 → 7632.8 | | | $(19^+) \rightarrow 17^+$ |
| 2356.7 | 23.4(3) | 5682.1 → 3325.4 | 1.77(18) | | $(15^+) \rightarrow 13^+$ |

[a]Uncertainties are between 0.2 and 0.5 keV depending upon their intensity.
[b]Intensities are normalized to the 2086.9-keV transition with $I_\gamma = 100$.
[c]Excitation energies of initial $E_i$ and final $E_f$ states.

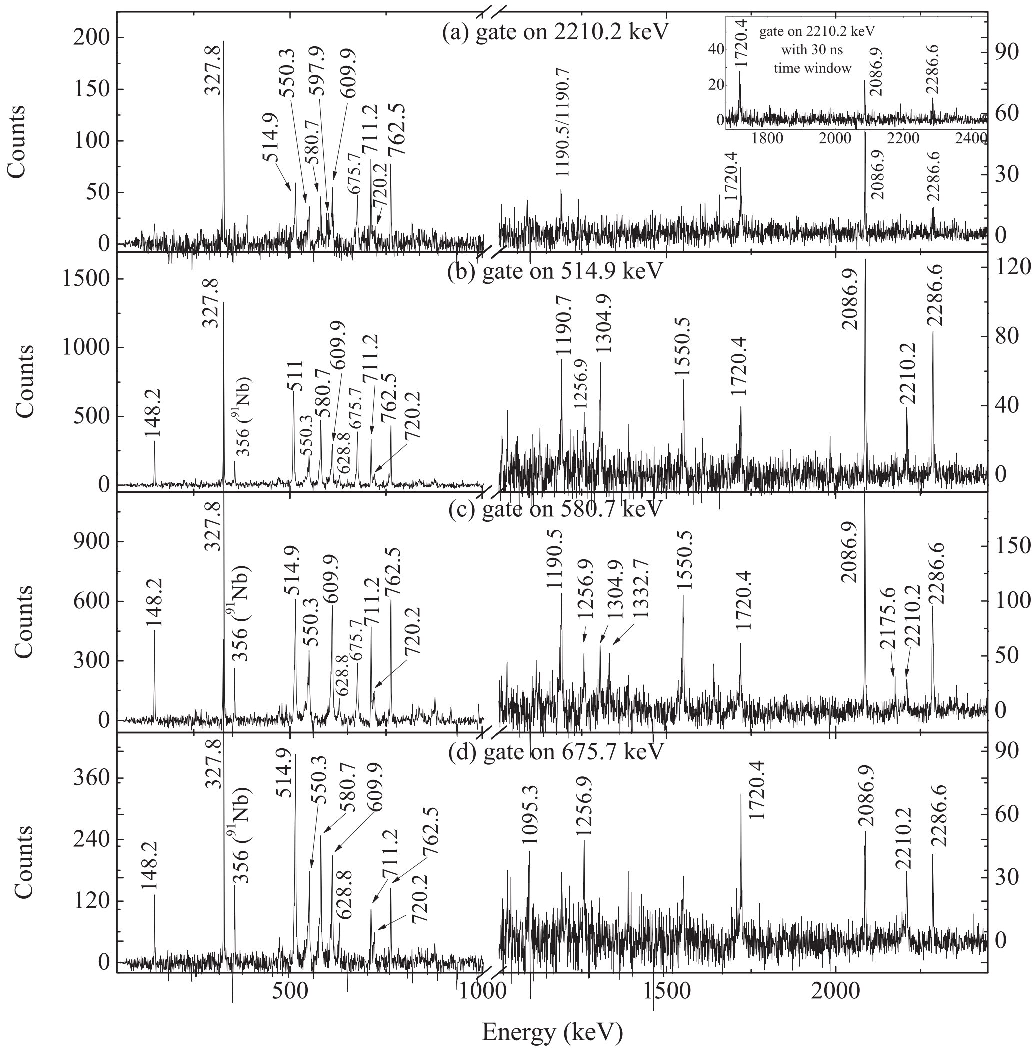

FIG. 2. Representative $\gamma$-$\gamma$ coincidence spectra gated on (a) 2210.2-, (b) 514.9-,(c) 580.7-, and (d) 675.7-keV transitions under selection on the 60 ns time window. The inset in (a) shows the same gated spectrum but selected on the 30 ns time window. Two different vertical scales were used for low- and high-energy $\gamma$ rays. The main coincidence $\gamma$ rays are labeled with energies in keV.

Each of these larger gaps appears to represent a change in the intrinsic structure. To check this hypothesis, calculations were performed by incorporating both the above-mentioned configurations originating from the proton excitation across the $Z = 38$ gap and the neutron excitation across the $N = 50$ shell closure.

## IV. DISCUSSION

The calculations for the low-lying states in the $N = 51$ isotones $^{89}$Sr [19], $^{90}$Y [21], $^{92}$Nb [3,45], $^{94}$Tc [42], $^{95}$Ru [13], by taking $^{88}$Sr as the core and the valence nucleons occupying the $(2p_{1/2}, 1g_{9/2})$ configuration space, were quite successful. However, the calculated energies of the states with higher spins are not in very good agreement with experimental results, and the description of states with higher spins is improved with an extended model space including the higher-lying neutron orbitals $1g_{7/2}$ and $2d_{5/2}$ as well as core excitation of the $1g_{9/2}$ neutron across the $N = 50$ shell closure into the $1g_{7/2}$ orbital [13,19,21,42]. Consequently, a model space that encompasses a large proton space and also allows for the excitation of a neutron across the $N = 50$ core would be expected to adequately describe the states with higher spins in these nuclei.

To interpret the decay sequences in $^{92}$Nb, spherical shell-model calculations were performed with the code NUSHELLX [46]. The GWB model space and GWBXG interaction are adopted in the code, and the model space includes four proton orbits $(1f_{5/2}, 2p_{3/2}, 2p_{1/2}, 1g_{9/2})$ and six neutron orbits $(2p_{1/2}, 1g_{9/2}, 1g_{7/2}, 2d_{5/2}, 2d_{3/2}, 3s_{1/2})$ relative to an inert $^{66}$Ni core. According to the reports in Refs. [18,20,47–49], the single-particle energies relative to the $^{66}$Ni core were set as $\varepsilon^{\pi}_{1f_{5/2}} = -5.322$ MeV, $\varepsilon^{\pi}_{2p_{3/2}} = -6.144$ MeV, $\varepsilon^{\pi}_{2p_{1/2}} = -3.941$ MeV, $\varepsilon^{\pi}_{1g_{9/2}} = -1.250$ MeV, $\varepsilon^{\nu}_{2p_{1/2}} = -0.696$ MeV, $\varepsilon^{\nu}_{1g_{9/2}} = -2.597$ MeV, $\varepsilon^{\nu}_{1g_{7/2}} = 5.159$ MeV, $\varepsilon^{\nu}_{2d_{5/2}} = 1.830$ MeV, $\varepsilon^{\nu}_{2d_{3/2}} = 4.261$ MeV, and $\varepsilon^{\nu}_{3s_{1/2}} = 1.741$ MeV. These single-particle energies and the corresponding values of the strengths of the residual interactions were used to calculate level energies.

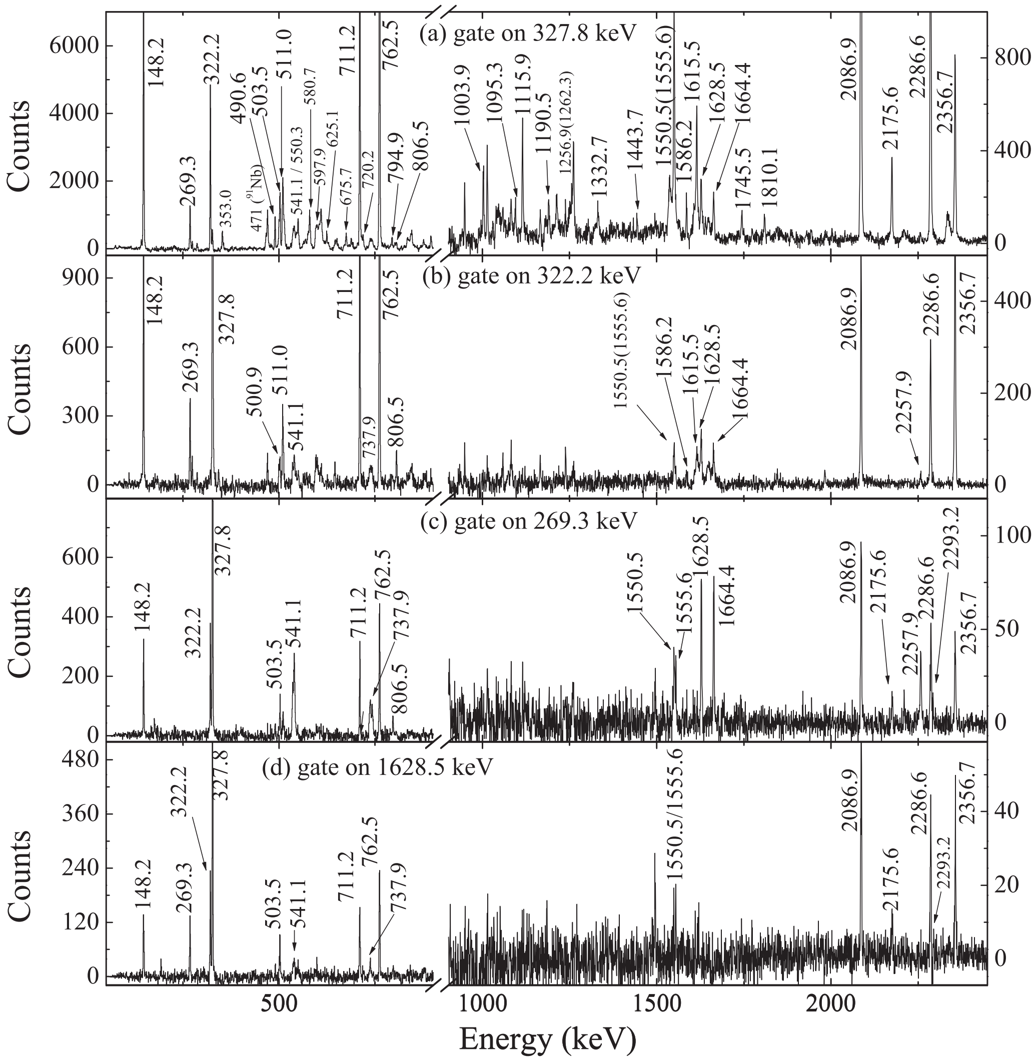


FIG. 3. Representative $\gamma$-$\gamma$ coincidence spectra gated on (a) 327.8-, (b) 322.2-, (c) 269.3-, and (d) 1628.5-keV transitions under selection on the 60 ns time window. Two different vertical scales were used for low- and high-energy $\gamma$ rays. The main coincidence $\gamma$ rays are labeled with energies in keV.

The nucleus $^{92}$Nb has 13 valence protons and 13 valence neutrons in the considered configuration space. Due to the large dimensions of the valence space, truncations were employed in our calculations for $^{92}$Nb. The valence protons are allowed to move freely among the $1f_{5/2}$, $2p_{3/2}$, $2p_{1/2}$, and $1g_{9/2}$ single-particle orbitals. Simultaneously, only one neutron was allowed to be excited from the low-energy orbital, $1g_{9/2}$, into the higher-energy $1g_{7/2}$ and $2d_{5/2}$ orbitals, as in the studies of $^{89}$Sr [19], $^{90}$Y [21], $^{94}$Tc [42], $^{95}$Ru [13], and so on. In addition, the valence neutron was allowed to be lifted from the $2d_{5/2}$ orbital to the $1g_{7/2}$ obital, but no neutrons were allowed to be excited to the $2d_{3/2}$ and $3s_{1/2}$ orbitals. The configurations of these higher-angular-momentum states are dominated by a neutron particle-hole excitation $\nu$ $(1g_{9/2}^{-1}, 1g_{7/2})$ coupled to the valence proton states in $fpg$ subspace. Calculated level energies in $^{92}$Nb are compared with experimental ones in Figs. 4 and 5. To investigate the structure properties of positive-parity and negative-parity sequences, the main partitions of the wave functions for each state are presented in Table II, characterized by two or three main configurations with larger contributions.

The high-spin states in $^{92}$Nb observed in the present work can be principally generated via four different mechanisms: (a) a proton pair excitations from the completely filled $2p_{1/2}$ orbits into the $1g_{9/2}$ orbits; (b) proton excitations from the completely filled $1f_{5/2}$, $2p_{3/2}$, $2p_{1/2}$ subshells into the $1g_{9/2}$ orbit. (c) valence neutron excitation from the $2d_{5/2}$ orbit into the $1g_{7/2}$ orbit; and (d) neutron particle-hole excitation $(1g_{9/2}^{-1}, 1g_{7/2})$ across the $N = 50$ shell closure. Each of these excitation mechanisms has been used to interpret the observed states of $^{92}$Nb.

The $I^{\pi} = 7^+$ ground state is predominantly generated by the coupling of one $1g_{9/2}$ proton to one unpaired neutron in the $2d_{5/2}$ orbital. The calculated excitation energies for the states with spin $I^{\pi} = 9^+, 11^+, 13^+, 14^+, 15^+$, and $16^+$ have reasonable agreement with the experiment results. The

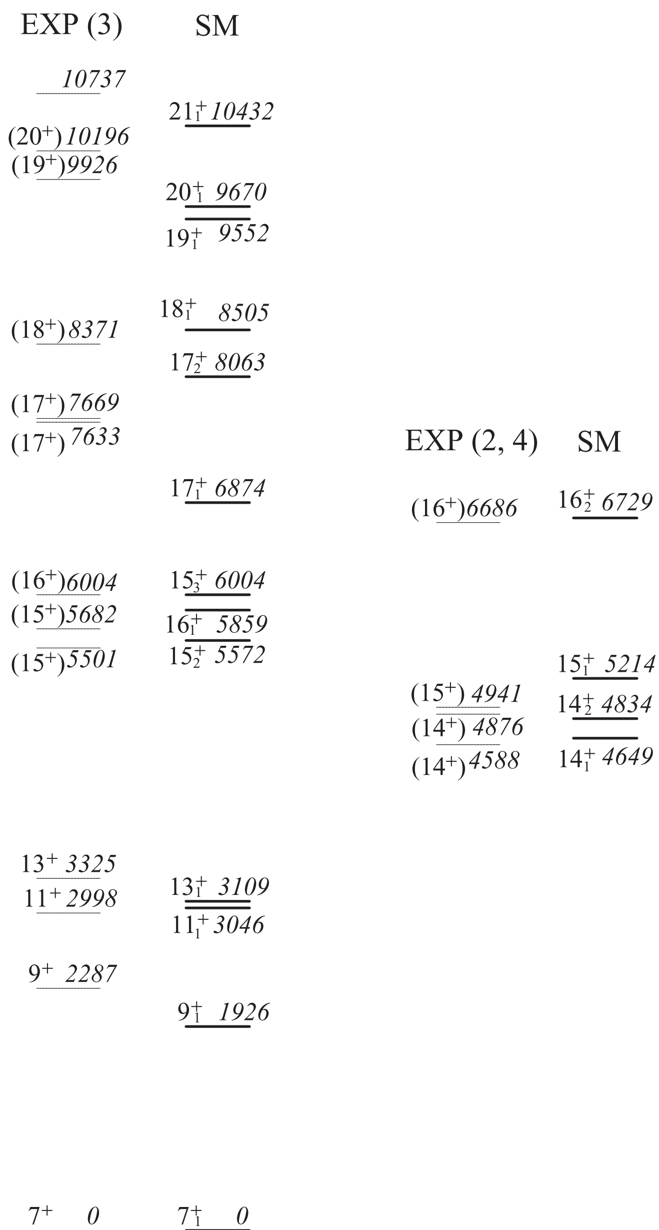


FIG. 4. Comparison of experimental excitation energies in $^{92}$Nb ($\pi = +$) with shell-model predictions with the model space GWB for proton orbits ($1f_{5/2}$, $2p_{3/2}$, $2p_{1/2}$, $1g_{9/2}$) and neutron orbits ($2p_{1/2}$, $1g_{9/2}$, $1g_{7/2}$, $2d_{5/2}$).

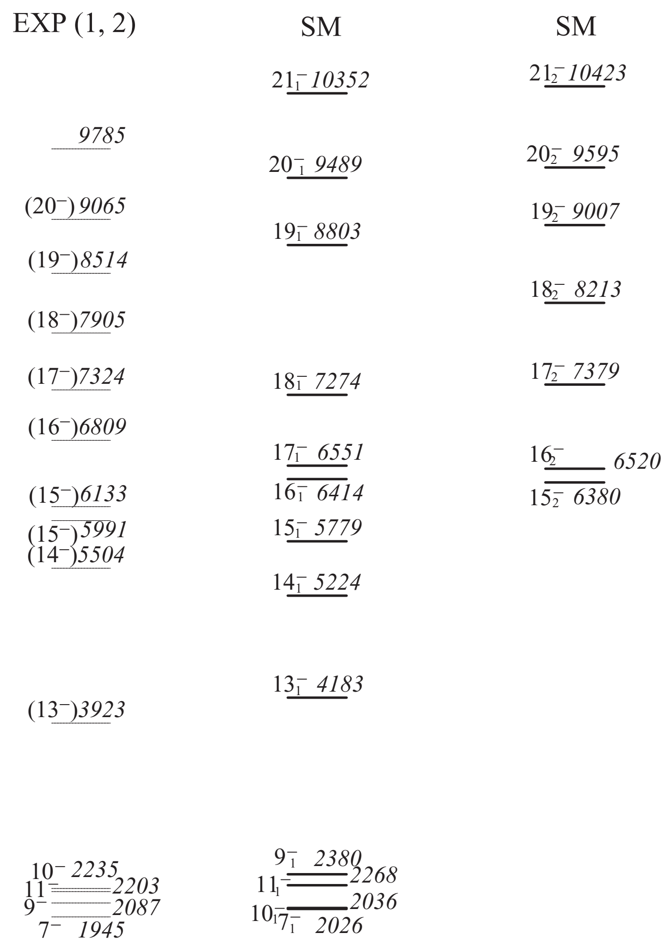


FIG. 5. Comparison of experimental excitation energies in $^{92}$Nb ($\pi = -$) with shell-model predictions with the model space GWB for proton orbits ($1f_{5/2}$, $2p_{3/2}$, $2p_{1/2}$, $1g_{9/2}$) and neutron orbits ($2p_{1/2}$, $1g_{9/2}$, $1g_{7/2}$, $2d_{5/2}$).

only point of disagreement is that the observed first $16^+$ state at energy of 6004 keV lies above the third $15^+$ state at energy of 5682 keV, but the calculation shows opposite results. The dominating contributions to the $9_1^+$, $11_1^+$, and $13_1^+$ states obtained in shell model arise from three protons at the $1g_{9/2}$ orbital coupling to one neutron at the $2d_{5/2}$ orbital. The contribution of the $\pi(1g_{9/2})^3 \otimes \nu(2d_{5/2})^1$ configuration up to the $13_1^+$ state is consistent with the calculated results of Ref [3]. The calculations predict that the yrast $14^+$ state has the same proton configuration as the $9_1^+$, $11_1^+$, and $13_1^+$ states; however, this yrast $14^+$ state also includes excitation of one neutron from the $2d_{5/2}$ into the $1g_{7/2}$ orbital. The yrare $14^+$ level at an energy of 4875.9 keV may correspond to the calculated state at an energy of 4834 keV, i.e., the $14_2^+$, which has the same neutron configuration as that of the $13_1^+$ state but involves proton excitation from the $1f_{5/2}$ and $2p_{3/2}$ orbitals to the $2p_{1/2}$ orbital.

The $15_1^+$, and $15_2^+$ states include the excitation of one proton over the shell gap at $Z = 38$ and into the $2p_{1/2}$ orbital. Consequently, a gap of about 2.1–2.5 MeV is predicted between the $13_1^+$ state and $15_1^+$ and $15_2^+$ states, respectively. Except for the $15_3^+$, the main configuration of the states from $15_1^+$ to $17_1^+$ is $\pi[(1f_{5/2})^{-1}(2p_{1/2})^1(1g_{9/2})^3] \otimes \nu(1g_{7/2}/2d_{5/2})^1$, as shown in Table II. The $16_1^+$, $16_2^+$, and $17_1^+$ states include the same proton configuration as the $15_1^+$ and $15_2^+$ states; however, these states are predicted to contain one neutron excitation from the $d_{5/2}$ orbital to the $g_{7/2}$ orbital. The $17_2^+$ state involves excitation of one proton from the $1f_{5/2}$ orbital to the $2p_{1/2}$ orbital. The experimentally observed state ($18^+$) with an energy of 8370.7 keV is well described by the configuration $\pi(1g_{9/2})^3 \otimes \nu[(1g_{9/2})^{-1}(1g_{7/2})^1(2d_{5/2})^1]$. Thus this state involves the neutron-core excitation $\nu[(1g_{9/2})^{-1}(1g_{7/2})^1]$. The $19_1^+$, $20_1^+$, and $21_1^+$ states may correspond to the experimental

TABLE II. Main partitions of the wave functions for $^{92}$Nb within the GWB model space. The wave function for a particular angular momentum state would be composed of several partitions. Each partition is of the form $p = \pi[p(1), p(2), p(3), p(4)] \otimes \nu[n(1), n(2), n(3), n(4)]$, where $p(i)$ represents the number of valence protons occupying the $1f_{5/2}$, $2p_{3/2}$, $2p_{1/2}$, and $1g_{9/2}$ orbits, and $n(j)$ represents the number of valence neutrons in the $2p_{1/2}$, $1g_{9/2}$, $1g_{7/2}$, $2d_{5/2}$ orbits. One neutron was allowed to be excited from $1g_{9/2}$ to the $g_{7/2}$ and $d_{5/2}$ orbitals, and no neutrons were allowed to be excited to the $2d_{3/2}$ and $3s_{1/2}$ orbitals in these calculations.

| $I^\pi$ ($\hbar$) | $E_{(\mathrm{exp})}$ (keV) | $E_{(\mathrm{cal})}$ (keV) | Wave function $\pi \otimes \nu$ | Seniority $\nu$ | Partitions (%) |
|---|---|---|---|---|---|
| $7_1^+$ | 0 | 0 | 6 4 2 1 $\otimes$ 2 10 0 1 | 2 | 37 |
| | | | 6 4 0 3 $\otimes$ 2 10 0 1 | 2 | 21 |
| $9_1^+$ | 2287 | 1926 | 6 4 0 3 $\otimes$ 2 10 0 1 | 4 | 30 |
| | | | 4 4 2 3 $\otimes$ 2 10 0 1 | 4 | 20 |
| $11_1^+$ | 2998 | 3046 | 6 4 0 3 $\otimes$ 2 10 0 1 | 4 | 43 |
| | | | 4 4 2 3 $\otimes$ 2 10 0 1 | 4 | 17 |
| $13_1^+$ | 3325 | 3109 | 6 4 0 3 $\otimes$ 2 10 0 1 | 4 | 45 |
| | | | 4 4 2 3 $\otimes$ 2 10 0 1 | 4 | 13 |
| $14_1^+$ | 4588 | 4649 | 6 4 0 3 $\otimes$ 2 10 1 0 | 4 | 48 |
| | | | 4 4 2 3 $\otimes$ 2 10 1 0 | 4 | 11 |
| | | | 6 3 1 3 $\otimes$ 2 10 1 0 | 6 | 10 |
| $14_2^+$ | 4876 | 4834 | 5 4 1 3 $\otimes$ 2 10 0 1 | 6 | 51 |
| | | | 5 3 2 3 $\otimes$ 2 10 0 1 | 6 | 22 |
| $15_1^+$ | 4941 | 5214 | 5 4 1 3 $\otimes$ 2 10 0 1 | 6 | 61 |
| | | | 5 3 2 3 $\otimes$ 2 10 0 1 | 6 | 21 |
| $15_2^+$ | 5501 | 5572 | 5 4 1 3 $\otimes$ 2 10 0 1 | 6 | 69 |
| $15_3^+$ | 5682 | 6004 | 6 3 1 3 $\otimes$ 2 10 0 1 | 6 | 47 |
| | | | 4 4 2 3 $\otimes$ 2 10 0 1 | 6 | 15 |
| $16_1^+$ | 6004 | 5859 | 5 4 1 3 $\otimes$ 2 10 1 0 | 6 | 73 |
| | | | 5 3 2 3 $\otimes$ 2 10 1 0 | 6 | 11 |
| $16_2^+$ | 6686 | 6729 | 5 4 1 3 $\otimes$ 2 10 1 0 | 6 | 61 |
| | | | 5 3 2 3 $\otimes$ 2 10 1 0 | 6 | 20 |
| $17_1^+$ | 7633 | 6874 | 5 4 1 3 $\otimes$ 2 10 1 0 | 6 | 75 |
| | | | 5 3 2 3 $\otimes$ 2 10 1 0 | 6 | 11 |
| $17_2^+$ | 7669 | 8063 | 4 4 2 3 $\otimes$ 2 10 0 1 | 6 | 44 |
| | | | 4 4 0 5 $\otimes$ 2 10 0 1 | 6 | 16 |
| $18_1^+$ | 8371 | 8505 | 6 4 0 3 $\otimes$ 2 9 1 1 | 6 | 38 |
| | | | 4 4 2 3 $\otimes$ 2 9 1 1 | 6 | 16 |
| $19_1^+$ | 9926 | 9552 | 6 4 0 3 $\otimes$ 2 9 1 1 | 6 | 34 |
| | | | 4 4 2 3 $\otimes$ 2 9 1 1 | 6 | 13 |
| $20_1^+$ | 10196 | 9670 | 6 4 0 3 $\otimes$ 2 9 1 1 | 6 | 34 |
| | | | 4 4 2 3 $\otimes$ 2 9 1 1 | 6 | 18 |
| $21_1^+$ | 10737 | 10432 | 5 4 1 3 $\otimes$ 2 9 1 1 | 8 | 70 |
| | | | 5 3 2 3 $\otimes$ 2 9 1 1 | 8 | 18 |

TABLE II. *(Continued.)*

| $I^\pi$ ($\hbar$) | $E_{(\mathrm{exp})}$ (keV) | $E_{(\mathrm{cal})}$ (keV) | Wave function $\pi \otimes \nu$ | Seniority $\nu$ | Partitions (%) |
|---|---|---|---|---|---|
| $7_1^-$ | 1945 | 2026 | 6 4 1 2 $\otimes$ 2 10 0 1 | 4 | 67 |
| $9_1^-$ | 2087 | 2380 | 6 4 1 2 $\otimes$ 2 10 0 1 | 4 | 41 |
| | | | 6 3 2 2 $\otimes$ 2 10 0 1 | 4 | 33 |
| $10_1^-$ | 2235 | 2036 | 6 4 1 2 $\otimes$ 2 10 0 1 | 4 | 65 |
| | | | 6 3 2 2 $\otimes$ 2 10 0 1 | 4 | 18 |
| $11_1^-$ | 2203 | 2268 | 6 4 1 2 $\otimes$ 2 10 0 1 | 4 | 74 |
| $13_1^-$ | 3923 | 4183 | 5 4 0 4 $\otimes$ 2 10 0 1 | 4 | 34 |
| | | | 5 4 2 2 $\otimes$ 2 10 0 1 | 4 | 29 |
| $14_1^-$ | 5504 | 5224 | 5 4 0 4 $\otimes$ 2 10 1 0 | 4 | 41 |
| | | | 5 4 2 2 $\otimes$ 2 10 1 0 | 4 | 8 |
| | | | 5 3 1 4 $\otimes$ 2 10 1 0 | 6 | 7 |
| $15_1^-$ | 5992 | 5779 | 5 4 0 4 $\otimes$ 2 10 0 1 | 6 | 49 |
| | | | 4 4 1 4 $\otimes$ 2 10 0 1 | 6 | 15 |
| | | | 5 3 1 4 $\otimes$ 2 10 0 1 | 6 | 15 |
| $15_2^-$ | 6133 | 6380 | 5 4 0 4 $\otimes$ 2 10 1 0 | 6 | 44 |
| | | | 4 4 1 4 $\otimes$ 2 10 1 0 | 6 | 16 |
| | | | 5 3 1 4 $\otimes$ 2 10 1 0 | 6 | 14 |
| $16_1^-$ | 6809 | 6414 | 5 4 0 4 $\otimes$ 2 10 0 1 | 6 | 49 |
| | | | 5 3 1 4 $\otimes$ 2 10 0 1 | 6 | 15 |
| $16_2^-$ | | 6520 | 5 4 0 4 $\otimes$ 2 10 1 0 | 6 | 47 |
| | | | 5 3 1 4 $\otimes$ 2 10 1 0 | 6 | 15 |
| | | | 4 4 1 4 $\otimes$ 2 10 1 0 | 6 | 15 |
| $17_1^-$ | 7324 | 6551 | 5 4 0 4 $\otimes$ 2 10 0 1 | 6 | 58 |
| | | | 5 3 1 4 $\otimes$ 2 10 0 1 | 8 | 16 |
| | | | 4 4 1 4 $\otimes$ 2 10 0 1 | 6 | 4 |
| $17_2^-$ | | 7379 | 5 4 0 4 $\otimes$ 2 10 0 1 | 6 | 55 |
| | | | 5 3 1 4 $\otimes$ 2 10 0 1 | 8 | 20 |
| | | | 4 4 1 4 $\otimes$ 2 10 0 1 | 6 | 5 |
| $18_1^-$ | 7905 | 7274 | 5 4 0 4 $\otimes$ 2 10 1 0 | 6 | 59 |
| | | | 5 3 1 4 $\otimes$ 2 10 1 0 | 8 | 23 |
| $18_2^-$ | | 8213 | 4 4 1 4 $\otimes$ 2 10 0 1 | 8 | 53 |
| | | | 4 3 2 4 $\otimes$ 2 10 0 1 | 8 | 24 |
| $19_1^-$ | 8514 | 8803 | 4 4 1 4 $\otimes$ 2 10 0 1 | 8 | 43 |
| | | | 5 3 1 4 $\otimes$ 2 10 0 1 | 8 | 15 |
| $19_2^-$ | | 9007 | 5 4 0 4 $\otimes$ 2 9 1 1 | 6 | 41 |
| | | | 5 4 2 2 $\otimes$ 2 9 1 1 | 6 | 16 |
| $20_1^-$ | 9065 | 9489 | 4 4 1 4 $\otimes$ 2 10 1 0 | 8 | 75 |
| | | | 4 3 2 4 $\otimes$ 2 10 1 0 | 8 | 13 |
| $20_2^-$ | | 9595 | 5 4 0 4 $\otimes$ 2 9 1 1 | 6 | 45 |
| | | | 5 4 2 2 $\otimes$ 2 9 1 1 | 6 | 13 |
| $21_1^-$ | 9785 | 10352 | 5 4 0 4 $\otimes$ 2 9 1 1 | 6 | 42 |
| | | | 5 4 2 2 $\otimes$ 2 9 1 1 | 8 | 14 |
| $21_2^-$ | | 10423 | 5 4 0 4 $\otimes$ 2 9 1 1 | 6 | 52 |
| | | | 5 3 1 4 $\otimes$ 2 9 1 1 | 8 | 17 |

levels at 9926.3, 10195.6, and 10736.7 keV, respectively. The high-energy positive parity states located above 10 MeV are linked by low-energy transitions. The calculation predicts that the $19_1^+$, $20_1^+$, and $21_1^+$ states have the same neutron-core excitation $\nu[(1g_{9/2})^{-1}(1g_{7/2})^1]$ as the $18_1^+$ state. In addition, the $21^+$ state also involves excitation of protons from the $1f_{5/2}$ or $2p_{3/2}$ orbital to the $2p_{1/2}$ orbital.

Regarding the negative states, the lowest-lying $7_1^-$, $9_1^-$, $10_1^-$, and $11_1^-$ states are well reproduced, with $\pi[(2p_{1/2})^1(1g_{9/2})^2)] \otimes \nu(2d_{5/2})^1$ configurations contributing maximally. The calculated $9_1^-$ state is predicted to be 344 and 112 keV higher than $10_1^-$ and $11_1^-$ states, respectively; however, the experimental $9^-$ level lies 148 and 116 keV lower than $10^-$ and $11^-$ levels. This calculated result is different from that of Ref. [3], in which the $10^-$ state is predicted to be higher than the $9^-$ and $11^-$ states. The $13_1^-$ state is generated by lifting two protons over the shell gap at $Z = 38$. Accordingly, a gap of about 1.9 MeV is predicted between the calculated $11_1^-$ and $13_1^-$ states, comparable with the energy of observed 1720.4-keV $\gamma$ ray. The observed $14^-$ level at an energy of 5504.0 keV may correspond to the calculated state at an energy of 5224 keV, i.e., the $14^-_1$ which has the same proton configuration as that of the $13^-_1$ state but involves neutron excitation from the $2d_{5/2}$ orbital to the $1g_{7/2}$ orbital. There are two $15^-$ states observed experimentally. The yrast $15^-$ state at an energy of 5992 keV could be described as a coupling of the unpaired $2d_{5/2}$ neutron with breakup a $1f_{5/2}$ proton pair and lifting one proton from the $1f_{5/2}$ and $2p_{1/2}$ orbitals to the $1g_{9/2}$ orbital, leading to the configuration $\pi[(1f_{5/2})^{-1}(1g_{9/2})^4] \otimes \nu(2d_{5/2})^1$. According to the calculation, the yrare $15^-$ state at an energy of 6133.2 keV is predicted to have the same configuration as that of the $14^-_1$ state.

As shown in Fig. 1, from $I^\pi = 16^-_1$ to $I^\pi = 20^-$, just one level is observed for each $I^\pi$. However, to better understand the structures of these high-spin negative parity states, two calculated states for each $I^\pi$ are given in Fig. 5 and Table II. The experimental $(16^-)$ state decays directly to the yrare $(15^-)$ state at 6133.2 keV, which is predicted to have the same intrinsic structure as the calculated $16^-_2$ state, i.e., $\pi[(1f_{5/2})^{-1}(1g_{9/2})^4] \otimes \nu(1g_{7/2})^1$ like the $15^-_1$ state. In fact, the energy of the $16^-_2$ state is 6520 keV, closer to the energy of the observed level than the calculated $16^-_1$ state. From the calculated results listed in Fig. 5 and Table II, the energy of the $17^-_2$ state is very close to the energy of the experimental level at 7323.8 keV; the difference is only 55 keV. So the $17^-$ state could be dominated by $\pi[(1f_{5/2})^{-1}(1g_{9/2})^4] \otimes \nu(2d_{5/2})^1$, mixing with $\pi[(1f_{5/2})^{-1}(2p_{3/2})^{-1}(2p_{1/2})^1(1g_{9/2})^4] \otimes \nu(2d_{5/2})^1$ and $\pi[(1f_{5/2})^{-2}(1g_{9/2})^4] \otimes \nu(2d_{5/2})^1$, the same as the yrast $15^-$ state. Experimentally, a $\gamma$ transition with an energy of 1332.7 keV connecting these two levels has been observed. Similarly, the $18^-_2$ state may correspond to the $I^\pi = (18^-)$ state at 7904.5 keV. This $18^-_2$ state is dominated by the $\pi[(1f_{5/2})^{-2}(1p_{1/2})^1(1g_{9/2})^4] \otimes \nu(2d_{5/2})^1$ configuration involving excitation of one proton from the $1f_{5/2}$ orbital to the $1p_{1/2}$ orbital. Although the calculated $19^-_1$ and $20^-_1$ states are about 290 and 424 keV higher than experimental ones, respectively, the energy difference of the calculated $20^-_1$ and $19^-_1$ states is 686 keV, which is close to the energy of the observed 550.3-keV $\gamma$ ray. The energy difference of the calculated $21^-_1$ and $20^-_1$ states is 863 keV, which is close to the energy of observed 720 keV $\gamma$ ray. Thus, the calculated $19^-_1$, $20^-_1$, and $21^-_1$ states might correspond to the experimental states at 8514.4, 9064.7, and 9784.9 keV respectively. Consequently, the $19^-$ state is also mainly dominated by the same configuration as that of the $18^-_2$ state. The $20^-$ state involves mainly one neutron excitation from the $d_{5/2}$ orbital to the $g_{7/2}$ orbital, i.e., a configuration of $\pi[(1f_{5/2})^{-2}(2p_{1/2})^1(1g_{9/2})^4] \otimes \nu(1g_{7/2})^1$. The level at 9784.9 keV, corresponding to the $21^-_1$ state, could be interpreted as the neutron-core excitation coupled a proton excitation, $\pi[(1f_{5/2})^{-1}(1g_{9/2})^4] \otimes \nu[(1g_{9/2})^{-1}(1g_{7/2})^1(2d_{5/2})^1]$.

The overall agreement of the observed states with those predicted by shell model calculations suggests that the excitations across the $N = 50$ shell gap do not play any significant role up to $I \approx 18\hbar$. However, the higher-spin levels above $I \approx 18\hbar$ are dominated by the neutron core excitation $(1g_{9/2}^{-1}, 1g_{7/2})$ and excitation of the protons over the shell gap at $Z = 38$ and into the $2p_{1/2}$ and $1g_{9/2}$ orbitals. In addition, for the lower-spin levels $I < 18\hbar$ in $^{92}$Nb, inspection of the wave functions reveals that the contribution of excitations from the proton $1f_{5/2}$ and $2p_{3/2}$ orbitals across the $Z = 38$ subshell cannot be ignored. It should be noted that the structure of sequence 1 at higher spin states shows features of collective motion. This is a possible reason for the poor agreement of observed states above $15^-$ in this sequence with calculated states.

## V. SUMMARY

High-spin states of $^{92}$Nb were populated via the reaction $^{82}$Se($^{14}$N, $4n$)$^{92}$Nb at a beam energy of 54 MeV. The previously reported level scheme of $^{92}$Nb has been extended considerably by adding nineteen new $\gamma$ rays and two new positive-parity decay sequences. Excited states in $^{92}$Nb were interpreted in the framework of the shell model. The calculations were performed in a model space including the $(1f_{5/2}, 2p_{3/2}, 2p_{1/2}, 1g_{9/2})$ orbitals for the protons and the $(2p_{1/2}, 1g_{9/2}, 1g_{7/2}, 2d_{5/2})$ orbitals for the neutrons. It is found that, to obtain a more appropriate description of the observed high-spin level structures, large-basis shell model calculations are necessary. The experimental high-spin levels could be interpreted by the configurations dominated by (i) the excitation of the protons over the $Z = 38$ proton core into higher orbitals, and (ii) the excitation of the neutron across the $N = 50$ neutron core into the next major oscillator shell. A detailed study of electromagnetic transition probabilities is required to give further insight into the exact nature of wave functions of these states.

## ACKNOWLEDGMENTS

The authors would like to thank the crew of the HI-13 tandem accelerator at the China Institute of Atomic Energy for steady operation of the accelerator and for preparing the target as well as Prof. Z. X. Li and Prof. Z. C. Gao for careful readings and useful discussions. This work is partially supported by the National Natural Science Foundation of China under Contracts No. U1867210, No. 11790322, No. 11575018, No. 11375023, No. 11305269, No. 11375267, and No. 11405274 as well as the Key Program of the Education Department of Anhui Province under Grant No. KJ2017A369.

[1] M. S. Zisman and B. G. Harvey, Phys. Rev. C **5**, 1031 (1972).
[2] B. A. Brown, P. M. S. Lesser, and D. B. Fossan, Phys. Rev. C **13**, 1900 (1976).
[3] B. A. Brown and D. B. Fossan, Phys. Rev. C **15**, 2044 (1977).
[4] C. Fields, J. Kraushaar, R. Ristinen, and L. Samuelson, Nucl. Phys. A **326**, 55 (1979).

[5] K. Muto, T. Shimano, and H. Horie, Phys. Lett. B **135**, 349 (1984).
[6] E. K. Warburton, J. W. Olness, C. J. Lister, R. W. Zurmühle, and J. A. Becker, Phys. Rev. C **31**, 1184 (1985).
[7] X. Ji and B. H. Wildenthal, Phys. Rev. C **37**, 1256 (1988).
[8] L. Funke, G. Winter, J. Döring, L. Käubler, H. Prade, R. Schwengner, E. Will, C. Protochristov, W. Andrejtscheff, L. Kostova *et al.*, Nucl. Phys. A **541**, 241 (1992).
[9] P. Singh, R. G. Pillay, J. A. Sheikh, and H. G. Devare, Phys. Rev. C **45**, 2161 (1992).
[10] S. S. Ghugre, S. B. Patel, M. Gupta, R. K. Bhowmik, and J. A. Sheikh, Phys. Rev. C **47**, 87 (1993).
[11] P. Singh, R. G. Pillay, J. A. Sheikh, and H. G. Devare, Phys. Rev. C **48**, 1609 (1993).
[12] H. A. Roth, S. E. Arnell, D. Foltescu, O. Skeppstedt, J. Blomqvist, A. Nilsson, T. Kuroyanagi, S. Mitarai, and J. Nyberg, Phys. Rev. C **50**, 1330 (1994).
[13] S. S. Ghugre, S. B. Patel, M. Gupta, R. K. Bhowmik, and J. A. Sheikh, Phys. Rev. C **50**, 1346 (1994).
[14] J. Reif, G. Winter, R. Schwengner, H. Prade, and L. Käubler, Nucl. Phys. A **587**, 449 (1995).
[15] S. S. Ghugre and S. K. Datta, Phys. Rev. C **52**, 1881 (1995).
[16] I. P. Johnstone and L. D. Skouras, Phys. Rev. C **55**, 1227 (1997).
[17] E. Stefanova, T. Kutsarova, I. Deloncle, M.-G. Porquet, M. Grinberg, E. Gueorguieva, T. Venkova, A. Minkova, F. Azaiez, S. Bouneau *et al.*, Nucl. Phys. A **669**, 14 (2000).
[18] E. A. Stefanova, R. Schwengner, J. Reif, H. Schnare, F. Dönau, M. Wilhelm, A. Fitzler, S. Kasemann, P. von Brentano, and W. Andrejtscheff, Phys. Rev. C **62**, 054314 (2000).
[19] E. A. Stefanova, R. Schwengner, G. Rainovski, K. D. Schilling, A. Wagner, F. Dönau, E. Galindo, A. Jungclaus, K. P. Lieb, O. Thelen *et al.*, Phys. Rev. C **63**, 064315 (2001).
[20] E. A. Stefanova, M. Danchev, R. Schwengner, D. L. Balabanski, M. P. Carpenter, M. Djongolov, S. M. Fischer, D. J. Hartley, R. V. F. Janssens, W. F. Mueller *et al.*, Phys. Rev. C **65**, 034323 (2002).
[21] G. Rainovski, R. Schwengner, K. D. Schilling, A. Wagner, A. Jungclaus, E. Galindo, O. Thelen, D. R. Napoli, C. A. Ur, G. de Angelis *et al.*, Phys. Rev. C **65**, 044327 (2002).
[22] N. S. Pattabiraman, S. N. Chintalapudi, S. S. Ghugre, B. V. Tirumala Rao, M. L. N. Raju, T. S. Reddy, P. K. Joshi, R. Palit, and H. C. Jain, Phys. Rev. C **65**, 044324 (2002).
[23] M. Hausmann, A. Jungclaus, E. Galindo, K. P. Lieb, O. Yordanov, I. P. Johnstone, R. Schwengner, A. Dewald, A. Fitzler, O. Möller *et al.*, Phys. Rev. C **68**, 024309 (2003).
[24] E. Galindo, M. Hausmann, A. Jungclaus, K. P. Lieb, O. Yordanov, I. P. Johnstone, R. Schwengner, A. Dewald, A. Fitzler, O. Möller *et al.*, Phys. Rev. C **69**, 024304 (2004).
[25] D. Bucurescu, Z. Podolyák, C. Rusu, G. d. Angelis, Y. H. Zhang, G. Căta Danil, I. Căta Danil, M. Ivaşcu, N. Mărginean, R. Mărginean *et al.*, Phys. Rev. C **71**, 034315 (2005).
[26] X. Z. Cui, L. H. Zhu, X. G. Wu, Z. M. Wang, C. Y. He, Y. Liu, G. S. Li, S. X. Wen, Z. L. Zhang, R. Meng *et al.*, Phys. Rev. C **72**, 044322 (2005).
[27] A. Chakraborty, Krishichayan, S. S. Ghugre, R. Goswami, S. Mukhopadhyay, N. S. Pattabiraman, S. Ray, A. K. Sinha, S. Sarkar, P. V. M. Rao *et al.*, Phys. Rev. C **72**, 054309 (2005).
[28] Y. Wakabayashi, T. Fukuchi, Y. Gono, A. Odahara, S. Tanaka, M. Inoue, T. Sasaki, M. Kibe, N. Hokoiwa, T. Shinozuka *et al.*, J. Phys. Soc. Jpn. **76**, 114202 (2007).
[29] D. Bucurescu, C. Rusu, N. Mărginean, C. A. Ur, G. d. Angelis, L. Corradi, D. Bazzacco, S. Beghini, F. D. Vedova, G. Duchene *et al.*, Phys. Rev. C **76**, 064301 (2007).
[30] C. Y. He, X. Z. Cui, L. H. Zhu, X. G. Wu, G. S. Li, Y. Liu, Z. M. Wang, S. X. Wen, H. B. Sun, R. G. Ma *et al.*, Chin. Phys. Lett. **27**, 028502 (2010).
[31] C. J. Xu, S. Y. Wang, C. Y. Niu, C. Liu, B. Qi, D. P. Sun, L. Liu, P. Zhang, Z. Q. Li, Z. Wang *et al.*, Phys. Rev. C **86**, 027302 (2012).
[32] S. Saha, R. Palit, J. Sethi, T. Trivedi, P. C. Srivastava, S. Kumar, B. S. Naidu, R. Donthi, S. Jadhav, D. C. Biswas *et al.*, Phys. Rev. C **86**, 034315 (2012).
[33] C. M. Baglin, Nucl. Data Sheets **114**, 1293 (2013).
[34] M. Bunce, P. H. Regan, V. Werner, C. W. Beausang, V. Anagnostatou, M. Bowry, R. J. Casperson, D. Chen, N. Cooper, P. M. Goddard *et al.*, Phys. Rev. C **87**, 044337 (2013).
[35] F. Ghazi Moradi, C. Qi, B. Cederwall, A. Ataç, T. Bäck, R. Liotta, M. Doncel, A. Johnson, G. de France, E. Clément *et al.*, Phys. Rev. C **89**, 014301 (2014).
[36] Y. H. Wu, J. B. Lu, P. W. Luo, G. S. Li, H. W. Li, X. G. Wu, C. Y. He, Y. Zheng, K. Y. Ma, D. Yang *et al.*, Chin. Phys. Lett. **31**, 042102 (2014).
[37] H. W. Li, J. B. Lu, G. S. Li, Y. Zheng, S. H. Yao, X. G. Wu, C. Y. He, Q. L. Xia, J. J. Liu, C. B. Li *et al.*, Chin. Phys. C **38**, 074004 (2014).
[38] P. W. Luo, X. G. Wu, H. B. Sun, G. S. Li, C. Y. He, Y. Zheng, C. B. Li, S. P. Hu, Y. H. Wu, H. W. Li *et al.*, Phys. Rev. C **89**, 034318 (2014).
[39] R. Schubart, A. Jungclaus, A. Harder, M. Kabadiyski, K. Lieb, D. Rudolph, M. Weiszflog, S. Albers, T. Burkardt, J. Eberth *et al.*, Nucl. Phys. A **591**, 515 (1995).
[40] P. Chowdhury, B. A. Brown, U. Garg, R. D. McKeown, T. P. Sjoreen, and D. B. Fossan, Phys. Rev. C **32**, 1238 (1985).
[41] W. F. Piel, D. B. Fossan, R. Ma, E. S. Paul, N. Xu, and J. B. McGrory, Phys. Rev. C **41**, 1223 (1990).
[42] S. S. Ghugre, S. Naguleswaran, R. K. Bhowmik, U. Garg, S. B. Patel, W. Reviol, and J. C. Walpe, Phys. Rev. C **51**, 2809 (1995).
[43] L. He, Y. H. Zhang, X. H. Zhou, M. L. Liu, Y. X. Guo, Z. G. Wang, B. Ding, Y. D. Fang, J. G. Wang, F. Ma *et al.*, Sci. Sinica Phys. Mech. Astron. **42**, 249 (2012).
[44] D. Radford, Nucl. Instrum. Methods Phys. Res., Sect. A **361**, 297 (1995).
[45] D. Gloeckner, Nucl. Phys. A **253**, 301 (1975).
[46] B. Brown and W. Rae, Nucl. Data Sheets **120**, 115 (2014).
[47] R. Gross and A. Frenkel, Nucl. Phys. A **267**, 85 (1976).
[48] J. Blomqvist and L. Rydström, Phys. Scr. **31**, 31 (1985).
[49] P. Li, W. Daehnick, S. K. Saha, J. Brown, and R. Kouzes, Nucl. Phys. A **469**, 393 (1987).